An Ultrasonic Imaging Speckle-Suppression and Contrast-Enhancement Technique by Means of Frequency Compounding and Coded Excitation

Jose R. Sanchez, *Student Member, IEEE*, and Michael L. Oelze, *Member, IEEE*

***Abstract*—A method for improving the contrast resolution of B-mode images is proposed by combining the speckle-reduction technique of frequency compounding (FC) and the coded-excitation and pulse-compression technique called resolution enhancement compression (REC). FC suppresses speckle but at the expense of a reduction in axial resolution. Using REC, the axial resolution and bandwidth of the imaging system was doubled. Therefore, by combining REC with FC (REC-FC), the tradeoff between axial resolution and contrast enhancement was extended significantly. Simulations and experimental measurements were conducted with a single-element transducer (f/2.66) having a center frequency of 2.25 MHz and a −3-dB bandwidth of 50%. Simulations and measurements of hyperechoic (+6 dB) tissue-mimicking targets were imaged. Four FC cases were evaluated: full-, half-, third-, and fourth-width of the true impulse response bandwidth. The image quality metrics used to compare REC-FC to conventional pulsing (CP) and CP-FC were contrast-to-noise ratio (CNR), speckle signal-to-noise ratio, histogram pixel intensity, and lesion signal-to-noise ratio. Increases in CNR of 121%, 231%, 302%, and 391% were obtained in experiments when comparing REC-FC for the full-, half-, third-, and fourth-width cases to CP. Furthermore, smaller increases in CNR of 112%, 233%, and 309% were obtained in experiments when comparing CP-FC for the half-, third-, and fourth-width cases to CP. Improved lesion detectability was observed by using REC-FC.**

I. Introduction

Speckle, the granular structure in ultrasonic images, reduces the ability to detect low-contrast targets. Speckle is formed by subresolution scatterers that cause constructive and destructive interference of backscattered ultrasonic signals within the resolution cell volume of an ultrasonic source [1]. Furthermore, speckle is considered to be a deterministic process because, when an object is imaged under the same operating conditions, no changes in the speckle pattern occur. Because of this nature, speckle is not reduced by signal averaging. Therefore, a considerable amount of work and effort has been spent over the last few decades developing techniques to reduce speckle in ultrasound images.

Manuscript received November 16, 2008; accepted April 15, 2009. This work was supported by a grant from the NIH (R21 EB006741).

The authors are with the Department of Electrical and Computer Engineering, University of Illinois at Urbana-Champaign, Urbana, IL (e-mail: jsanch27@uiuc.edu).

Digital Object Identifier 10.1109/TUFFC.2009.1189

In imaging, small structures or an object could be identified if the contrast between the target and the surrounding area are different [2]. In ultrasound, the difference in contrast between different soft tissues could be as small as 1%. Therefore, by using speckle-reduction techniques, image contrast can be improved by removing the interference pattern created by speckle, which is also known as speckle noise, and enhance the detectability of structures with low contrast from the background [3]. Consequently, speckle-reduction techniques have been used clinically and applied to commercial systems to improve the ability to detect small structures and lesions.

Speckle-reduction techniques can be classified into 2 categories: postprocessing techniques and compounding methods. Examples of some of the postprocessing techniques are adaptive filtering (linear and nonlinear) [4]–[8], deconvolution [9], [10], and wavelet despeckling [11], [12]. The compounding speckle-reduction methods include spatial and frequency compounding. These schemes rely on making separate images that have uncorrelated or partially correlated speckle patterns and then are averaged to reduce the speckle but at the expense of spatial resolution. Originally for spatial compounding, the source aperture was translated laterally or at different angles to make images from different orientations [13], [14]. The main drawbacks of these techniques are loss in lateral resolution and image alignment due to motion that causes image artifacts. Also, the need for multiple images would mean a decrease in the frame rate. Recently, however, manufacturers have employed receive aperture-only spatial compounding that is not subject to frame rate losses or motion-based image registration errors. Other advances in spatial-compounding [15], [16] use electronic-beam steering to obtain images at different angles and to overcome some of these tradeoffs by using advanced image registration.

Another method, known as frequency compounding (FC), can be applied on transmit mode by using multiple sources at different frequencies or on receive mode as a postprocessing speckle-reduction technique by dividing the spectrum of the radio-frequency (RF) echoes into subbands to make separate images [17]–[23]. The latter instance is also known as frequency diversity [18], [23], or split spectrum processing [21]. The main disadvantage introduced by using frequency compounding is the inherent tradeoff between axial and contrast resolution. Consequently, if the axial resolution and the bandwidth of

an ultrasonic imaging system could be increased, these tradeoffs between axial and contrast resolution could be extended. The first researchers that applied FC to medical ultrasound were Abbott and Thurstone [17]. In this study, they compared laser speckle to ultrasound speckle and suggested several techniques to generate independent speckle patterns including FC. Magnin *et al.* [19] observed that decorrelation of speckle patterns is dependent on the excitation bandwidth and obtained increases in speckle signal-to-noise ratio (sSNR) of 26% in B-mode images using a phased array system. Melton *et al.* [20] developed a model to predict the amount of speckle reduction in A-mode scans based on correlation coefficients. Trahey *et al.* [14] discussed a method for optimal speckle reduction based on the number of images that should be acquired within the available system bandwidth. Gehlbach *et al.* [18] studied frequency diversity using digital filtering techniques to determine a method to maximize sSNR and increase the ability to detect low-contrast targets. In addition, it was observed that a 10 to 15% increase in sSNR could be achieved by increasing the number of filters and filter overlap. Stetson *et al.* [24] used frequency-diversity techniques with the combination of gray-level mapping to improve the contrast-to-noise ratio (CNR) of low-contrast targets.

A recently developed coded excitation and pulse compression technique—resolution enhancement compression (REC)—enables enhancement of the axial resolution and bandwidth of the imaging system [25]. In addition to improvements in terms of axial resolution, the REC technique has the typical coded excitation and pulse compression benefits, such as deeper penetration due to improvement in echo signal-to-noise ratio (eSNR). Therefore, the goal of this study was to combine the REC technique with FC, which will be described as REC-FC, to extend the tradeoff of loss in axial resolution versus enhancement in contrast.

II. Problem Formulation

The driving force behind the REC technique [25] is the capability to shape and select to a limited degree certain desired characteristics of an ultrasonic imaging system through coded excitation and pulse compression. Consequently, the characteristics of the impulse response of the imaging system could be tailored to have useful properties for particular imaging applications. For example, if the usable bandwidth of the imaging system could be increased using REC, the increase in bandwidth could be used with FC to improve target contrast while retaining the original axial resolution of the imaging system.

In REC, a preenhanced chirp is used to excite an ultrasonic source selectively with different energies at chosen frequencies. Using the concept of convolution equivalence in the frequency domain as described in [25], a preenhanced chirp can be found by applying the following equation,

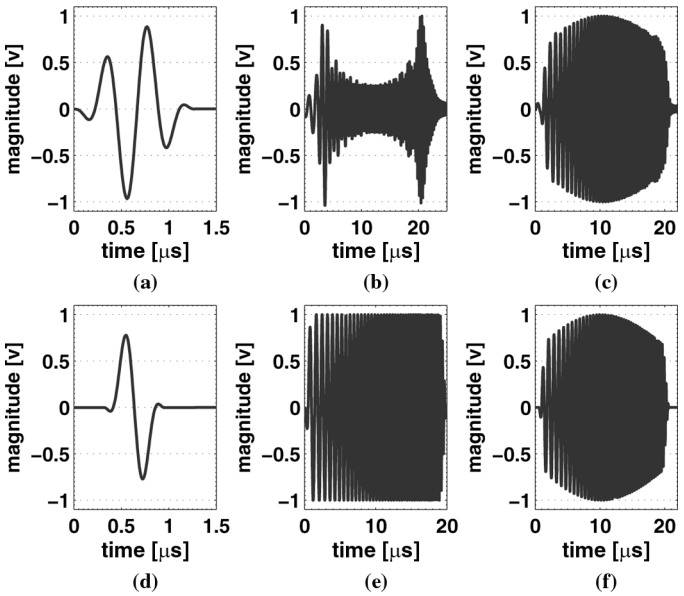

Fig. 1. Convolution equivalence from simulations: (a) pulse-echo impulse response with a 50% −3-dB bandwidth, (b) pre-enhanced chirp used to excite the 50% source, (c) convolution of 50% source with pre-enhanced chirp, (d) pulse-echo impulse response with a 100% −3-dB bandwidth, (e) linear chirp used to excite the 100% source, and (f) convolution of 100% source with linear chirp.

$$V_{\mathrm{pre}}(f) = \frac{H_1^*(f)}{|H_1(f)|^2 + |H_1(f)|^{-2}} \cdot H_2(f) \cdot V_{\mathrm{lin}}(f), \quad (1)$$

where $H_1(f)$ is the Fourier spectrum of the pulse-echo impulse response, $H_2(f)$ is the Fourier spectrum of the desired response, and $V_{\mathrm{lin}}(f)$ is the Fourier spectrum of a linear chirp. A time-domain example of the convolution equivalence is illustrated in Fig. 1. By exciting the transducer with the preenhanced chirp, the bandwidth is enhanced due to the increase of energy in the frequency bands that normally would be filtered in some measure by the bandpass nature of the transducer. Conceptually, to obtain a constant eSNR per frequency channel across the desired bandwidth, the additional amount of energy required on transmit at the outer frequency bands will depend on the original transducer's bandwidth and the amount of bandwidth boost desired. For example, if a source with a –6-dB bandwidth of 50% is boosted 100%, up to and more than twice as much energy can be pumped into the inefficient bands compared with the center frequency of the source.

After exciting the source with a preenhanced chirp, the received signal is compressed using a Wiener filter based on convolution equivalence. The resulting backscattered signal has an impulse response $h_2(t)$. Wiener filtering is described by the following equation:

$$\beta_{\mathrm{REC}}(f) = \frac{V_{\mathrm{lin}(f)}^{'*}}{|V_{\mathrm{lin}}^{'}(f)|^2 + \gamma \cdot \overline{\mathrm{eSNR}}^{-1}(f)}, \quad (2)$$

where $V_{\mathrm{lin}}^{'}(f)$ is the Fourier spectrum of a modified linear chirp, γ is a smoothing parameter that allows tradeoff

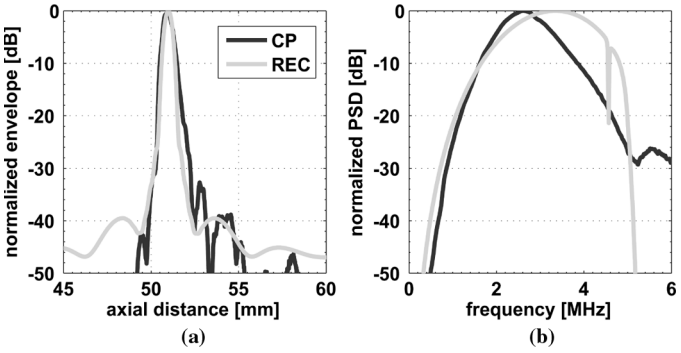

Fig. 2. (a) Simulated envelope from a point scatterer in an attenuated media and (b) power spectral density for conventional pulsing (CP) and the resolution enhancement compression (REC) compressed waveforms.

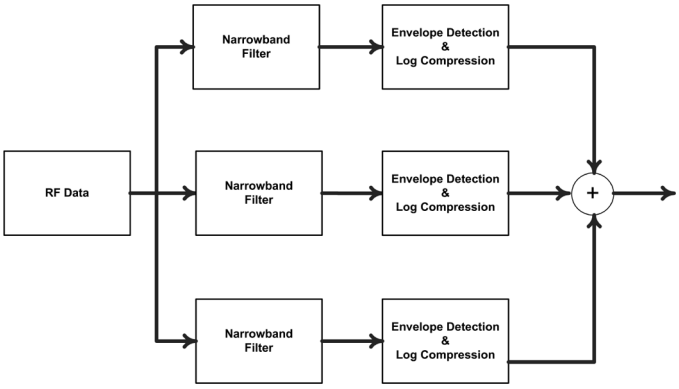

Fig. 3. Block diagram of a frequency compounding scenario with 3 subbands.

between axial resolution, gain in eSNR, and sidelobe levels. A modified linear chirp is used to restore convolution equivalence as the signal is slightly altered and filtered by electronics. eSNR [26] is the average eSNR per frequency channel and is defined as:

$$\overline{\mathrm{eSNR}}(f) = \frac{|\, H_{2c}(f)\,|^2 \cdot E\{|\, F(f)\,|^2\}_f}{E\{|\, \eta(f)\,|^2\}_\eta}, \tag{3}$$

where $|F(f)|^2$ is the power spectral density (PSD) of the object function, $|\eta(f)|^2$ is the PSD of the noise, and $|H_{2c}(f)|^2$ is the PSD of the ensemble average of the compressed signal over noise, $h_{2c}(t)$, which is defined as

$$h_{2c}(t) = E\{g(t)\}_{\text{noise}}, \tag{4}$$

where $E\{\ \}$ is the expected value of the argument and $g(t)_{\text{noise}}$ is the compressed signal over noise.

The envelope of the REC waveform (impulse response with double bandwidth) reflected from a point scatterer in an attenuated media (0.5 dB/cm/MHz) at an axial distance of 50 mm and the envelope for conventional pulsing (CP) methods are shown in Fig. 2(a). The PSD of REC waveform and CP methods are shown in Fig. 2(b) to illustrate the bandwidth enhancement that was achieved by using the REC technique.

The objective of using FC is to reduce the speckle noise and enhance the contrast in ultrasonic B-mode images. In FC, the received wideband RF spectrum is partitioned into N subbands by using Gaussian band-pass filters of smaller bandwidth than the original spectrum. These narrowband subbands create separate images that make partially uncorrelated speckle patterns, up to 60% decorrelation [19]. Typically, improvements in sSNR and CNR are proportional to $\sqrt{N}$; however, because these separate images are partially correlated, the improvements are going to be proportional to a factor less than the square root of the sum of uncorrelated images [1]. These separate images can then be added together to reduce the speckle by reducing the image intensity variance. However, the axial resolution deteriorates because the compounded image was generated by averaging smaller subband images. A block diagram shown in Fig. 3 depicts the operation of FC for a system of $n = 3$.

By using REC, a larger bandwidth is available, which would allow an increase in the number of subbands that can be applied for a particular desired axial resolution. Accordingly, a parameter of interest would be the bandwidth of these subbands. Therefore, in simulations and experiments, 4 cases were evaluated in terms of the subband bandwidth when applying FC to the REC technique. The first case consisted of using subbands that are full-width of the true impulse response bandwidth. This will gauge the true benefits of using the REC-FC technique because the resolution of the compounded image will be the same as that for CP methods and the contrast resolution will improve due to FC. Other cases will consist of using subbands smaller than the full-width, specifically, half-, third-, and fourth-width of impulse response bandwidth. A plot showcasing the size of the subbands for all cases in addition to the original bandwidths of CP and REC is shown in Fig. 4. The cases of genuine interest are full- and half-width because the intention of this work is to improve the contrast without suffering a large amount of resolution loss. However, for study completion, the later 2 cases also evaluated third- and fourth-width. In addition, for the last 3 cases, FC will be applied to CP (CP-FC) for comparison purposes. Other filter bank parameters that were considered when applying FC to the RF spectrum were subband center frequency separation, first subband center frequency starting point, and the number of subbands. The values of these parameters, which were chosen because they optimized the image quality metrics, are defined in the following paragraphs.

To evaluate the performance of the REC-FC technique compared with CP and CP-FC the following image quality metrics were used:

1. Contrast-to-noise ratio (CNR): CNR [3], also known as contrast-to-speckle ratio, is a quantitative measure that will assess image quality and describe the ability to perceive a target from the background region. CNR is defined as

$$\mathrm{CNR} = \left| \frac{\mu_B - \mu_T}{\sqrt{\sigma_B^2 + \sigma_T^2}} \right|, \tag{5}$$

where μ_B and μ_T are the mean brightness of the background and the target lesion and σ_B^2 and σ_T^2 are the variance of the background and target, respectively. To avoid possible errors in the calculations due to attenuation, the evaluated regions of interest in the background and the target lesion will be of the same size (900 × 20 samples, axially and laterally) and are located at the same depth.

2. Speckle signal-to-noise ratio (sSNR): sSNR [27] is a measure of the fluctuations in the speckle of a particular region of interest and is defined as

$$\mathrm{sSNR} = \frac{\mu}{\sigma}, \tag{6}$$

where μ and σ are the mean and the standard deviation of the region of interest, respectively. Specifically, sSNR will be evaluated for same-sized regions (900 × 20 samples, axially and laterally) in the target lesion and the background that are located at the same depth. For Rayleigh statistics, sSNR is equal to 1.91 [1].

3. Histogram pixel intensity (HPI): HPI is the mean of the frequency distribution of gray-scale pixel intensities and is described by

$$\mathrm{HPI} = E\{B\}. \tag{7}$$

B is the histogram being evaluated and is described by

$$B(i) = c_i, \tag{8}$$

where c_i represents the number of pixels in the image within a particular intensity level, i, which is an integer between 0 and 255 that represents the gray-scale levels used in B-mode images. Histograms will be made for same-sized regions (900 × 20 samples, axially and laterally) for the target lesion and the background and located at the same depth. Ideally, for superior target detectability, there is no overlap present between the target histogram and the background histogram. Therefore, histogram overlap (HO) the percentage of overlapping pixels between these 2 regions will be considered as well.

4. Lesion signal to noise ratio (lSNR): lSNR [27] is a ratio of contrast-detail and resolution. Contrast detail is an analytical measurement of image quality that quantifies the ability of the observer/imaging device to detect an isolated object of minimum size at a fixed contrast, at a given level of observer confidence, and for a given noise level [28]. The lSNR relation is defined as

$$\mathrm{lSNR} = \frac{C \cdot d \cdot \sqrt{N}}{\sqrt{S_{cx} \cdot S_{cz}}}, \tag{9}$$

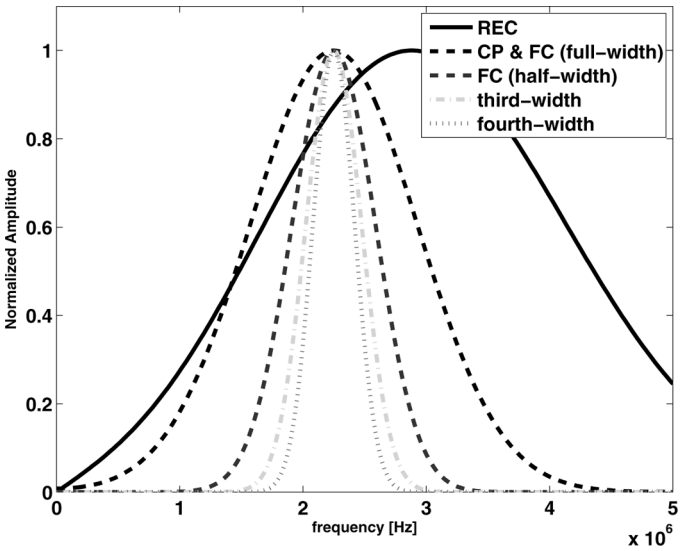

Fig. 4. Illustration of the bandwidth for all 4 frequency compounding (FC) cases applied in conjunction with the bandwidth of the reference signals for conventional pulsing (CP) and resolution enhancement compression (REC). Note: REC center frequency was shifted to eliminate any dc-component in the spectrum.

where d is the diameter of the target lesion, N is the number of uncorrelated images generated with FC ($n = 1$ otherwise), S_{cx} and S_{cz} are the average cell size in the lateral and axial direction, respectively, and C [28] is the contrast of the target and is defined by

$$C = \frac{\psi_1 - \psi_2}{\sqrt{\psi_1 + \psi_2}}, \tag{10}$$

where ψ_1 and ψ_w are the mean-square scattering strength (backscatter intensity) of the background and the target lesion, respectively. The average cell size is obtained using the normalized autocovariance function [29]. It is noteworthy to state that although the correlation function can be evaluated for the compounded image, the results generated are inaccurate because the uncorrelated speckle patterns are averaged, which would morph the speckle size. As a result, the average correlation function was evaluated by using one of the subband images generated.

III. Computer Simulations and Results

Computer simulations were carried out in Matlab (MathWorks, Natick, MA) to characterize the performance of the REC-FC technique. The simulations used a received pulse-echo pressure field model [30] described as

$$g'(x,y,t) = h_1(t) * f(x,y) * h_{\mathrm{pe}}(y,t), \tag{11}$$

where x represents the axial spatial coordinate, y represents the lateral spatial coordinate, $h_1(t)$ is the pulse-echo impulse response of the transducer, $f(x,y)$ is the scattering

function, and $h_{\mathrm{pe}}(y,t)$ is the modified pulse-echo spatial impulse response that takes into consideration the geometry of the transducer to the spatial extent of the scattered field (beam diffraction). The pulse-echo impulse response, $h_1(t)$, for CP was generated by gating a sinusoid of 4-cycles with a Hanning window

$$w(n) = \begin{cases} 0.5 \cdot \left(1 - \cos\left(\dfrac{2\pi n}{L_H - 1}\right)\right), & 0 \le n \le L_H - 1 \\ 0, & \text{otherwise} \end{cases} \tag{12}$$

where n is an integer and L_H is the number of samples in the window. The window and sinusoid parameters were chosen such that they match the transducer used in experiments. As a result, the pulse-echo impulse response generated is located at the focus of a 2.25-MHz single-element transducer (f/2.66) with a fractional bandwidth of 50% at −3 dB, which would correspond to a window length of $n = 128$. For REC, the desired impulse response function, $h_2(t)$, was constructed to have double the fractional bandwidth or 100% at −3 dB, compared with CP method; therefore, a Hanning window of size of half the length, $n = 64$, was used. The spatial response for a circular focused piston source can be simulated as a circular Gaussian beam that is defined as

$$h_{\mathrm{pe}}(y,t) = \delta\left(t - \frac{2R_d}{c}\right) e^{-y^2/\sigma_y^2}, \tag{13}$$

where R_d is the distance from the source to target in space, c is the speed of sound of the medium, and σ_y, which is equal to 1.28 mm, is the nominal lateral beamwidth of the source at −6 dB.

The received RF backscatter data were sampled at a rate of 100 MHz and the transducer was translated laterally in increments of 0.1 mm. The received RF data have a size of 4096 × 58 samples, axially and laterally. The object being imaged was a simulated phantom that was 20 mm long, 30 mm wide, and 1.92 mm high. A cylindrical target with a radius of 7.5 mm was located at the center of the phantom. To generate a hyperechoic target with a contrast of approximately +6 dB and the amplitude of the scatterers in the target lesion region was twice of the amplitude at the background. To achieve fully developed speckle, the phantom contains an average of 20 point scatterers per resolution cell volume. The scatterers were uniformly distributed throughout the phantom.

Fifty phantoms were simulated and evaluated with the image quality metrics discussed in Section II. Attenuation and noise were not modeled in the simulations to examine the relationship of FC to speckle effect only. In simulations, no optimization of the γ parameter in the Wiener filter (2) was used. However, in this study the γ parameter was determined by adjusting the parameter until it forced the Wiener filter toward an inverse filter to increase the axial resolution but not far enough that it would increase the noise above the background speckle level. A description of the filter banks designed along with the resolution needed to calculate lSNR in (9) are shown in Table I. In addition, the CNR, sSNR, HPI, HO, and lSNR results obtained for all 4 cases (full-, half-, third-, and fourth-width) in addition to the reference scans (CP and REC with no compounding) are summarized in Table II. The improvements in terms of CNR, sSNR_B, and sSNR_T are shown in Figs. 5(a)–(c). The B-mode images representing these results are displayed in Fig. 6.

Examination of the reference scans in Fig. 6(a) reveals that, by using the REC technique, the speckle size is finer when compared with CP. This smaller speckle size obtained by using REC means that the object boundaries would be more defined because there is more detail compared with CP. This resolution boost was then traded away to improve contrast by applying FC with subbands that have the same bandwidth as CP (full-width) as shown in Fig. 6(b). For the full-width case, the CNR, sSNR_B, and sSNR_T improved by a factor of 71%, 53%, and 51% when compared with CP. Essentially, a gain of CNR and sSNR was achieved while maintaining the same resolution that would be obtained by using CP methods. Examination of Fig. 5(d) suggests that by applying REC-FC the target was more detectable than using CP methods. The lSNR for REC was increased by a factor of 15% when compared with CP. This would imply that the same lSNR value would be obtained for both CP and REC if a target of approximately 13 mm in diameter were imaged with REC rather than 15 mm as in CP.

In addition to improvements in contrast, the boundaries of the target were more pronounced with REC-FC when compared with CP. This edge enhancement was due to the resolution enhancement in the REC reference image, which led to an increased amount of detail as shown in Fig. 7. The images generated in Fig. 7 were generated by applying a −6-dB threshold on the envelopes of CP, REC, and REC-FC (full-width) and then estimating the margin strength [31]. The difference in contrast between the background and the target was 6 dB; therefore, a threshold of −6 dB was considered. A threshold was applied to segment the target from the background, i.e., pixel values greater than −6 dB are considered part of the target and were assigned a value of one while all other pixel values were assigned a value of zero. Margin strength was then estimated to detect the strength of the distinct boundaries generated by applying the −6-dB threshold. Margin strength [31] is defined by the following equation:

$$\mathrm{MS} = E\left\{\sqrt{\left(\frac{d\mathrm{ROI}}{dx}\right)^2 + \left(\frac{d\mathrm{ROI}}{dy}\right)^2}\right\}, \tag{14}$$

where ROI is the region-of-interest within the envelope. From estimates of the margin strength, shown in Fig. 7, the target's edge was clearly defined and outlined for REC-FC when compared with CP. For REC this was not the case; however, when carefully examining REC versus CP, it was evident that REC had less background content around the target edges when compared with CP, allowing the boundaries to be traced.

TABLE I. FILTER BANK DESCRIPTIONS, AXIAL AND LATERAL CORRELATION FUNCTIONS FOR THE 50 CASES OF SIMULATED RF DATA FOR A 15-MM TARGET.

		Filter Banks			Resolution[1]	
Technique[2]	Description	Bandwidth (MHz)	Separation (MHz)	Quantity	Axial (mm)	Lateral (mm)
CP	Reference scan	—	—	—	0.30 ± 0.03	1.27 ± 0.44
REC	Reference scan	—	—	—	0.20 ± 0.01 (33%)	1.37 ± 0.49 (8%)
REC-FC	Full width of CP BW[3]	1.1	1.3	3	0.44 ± 0.05 (47%)	1.70 ± 0.57 (34%)
CP-FC	1/2 width of CP BW	0.6	0.6	4	0.82 ± 0.13 (169%)	1.66 ± 0.65 (31%)
REC-FC	1/2 width of CP BW	0.6	0.6	7	0.89 ± 0.16 (194%)	1.78 ± 0.54 (40%)
CP-FC	1/3 width of CP BW	0.4	0.4	6	1.17 ± 0.23 (285%)	1.70 ± 0.49 (34%)
REC-FC	1/3 width of CP BW	0.4	0.4	10	1.37 ± 0.32 (351%)	1.76 ± 0.50 (39%)
CP-FC	1/4 width of CP BW	0.3	0.3	8	1.48 ± 0.29 (386%)	1.70 ± 0.53 (34%)
REC-FC	1/4 width of CP BW	0.3	0.3	13	1.77 ± 0.39 (485%)	1.74 ± 0.51 (37%)

[1]The resolution values in the table are described in terms of the mean plus/minus one standard deviation. Values in parentheses represent the absolute percent change of REC-FC vs. CP reference.
[2]CP = conventional pulsing; REC = resolution enhancement compression; FC = frequency compounding.
[3]BW = bandwidth.

TABLE II. CNR, SSNR, HPI, HO, AND LSNR FOR THE 50 CASES OF SIMULATED RF DATA FOR A 15-MM TARGET.[1]

Technique[2]	Description	CNR	$sSNR_B$	$sSNR_T$	HPI_B	HPI_T	HO (%)	lSNR
CP	Reference scan	0.74 ± 0.14	1.94 ± 0.11	1.90 ± 0.11	169.3 ± 28.1	199.0 ± 28.6	28	15.86 ± 2.80
REC	Reference scan	0.74 ± 0.10 (0%)	1.94 ± 0.10 (0%)	1.89 ± 0.08 (0%)	165.3 ± 27.9 (3%)	194.9 ± 28.4 (2%)	28	18.21 ± 3.00 (15%)
REC	Full width of CP BW[3]	1.27 ± 0.17 (71%)	2.98 ± 0.24 (53%)	2.87 ± 0.19 (51%)	181.5 ± 16.3 (5%)	211.3 ± 16.7 (5%)	18	18.77 ± 3.62 (18%)
CP	1/2 width of CP BW	1.41 ± 0.26 (89%)	3.22 ± 0.33 (65%)	3.05 ± 0.27 (60%)	187.6 ± 14.9 (0%)	217.7 ± 15.3 (9%)	16	15.85 ± 3.32 (0%)
REC	1/2 width of CP BW	1.77 ± 0.23 (137–25%)	3.97 ± 0.36 (103–23%)	3.71 ± 0.32 (95–22%)	192.1 ± 11.8 (10–10%)	222.1 ± 12.1 (10–1%)	10	18.29 ± 3.51 (15–15%)
CP	1/3 width of CP BW	1.73 ± 0.31 (133%)	3.88 ± 0.49 (99%)	3.44 ± 0.35 (81%)	194.4 ± 12.1 (0%)	224.5 ± 12.6 (6%)	11	15.55 ± 3.06 (2%)
REC	1/3 width of CP BW	2.14 ± 0.30 (187–24%)	4.77 ± 0.60 (144–23%)	4.08 ± 0.38 (114–18%)	196.8 ± 10.0 (1–1%)	227.6 ± 10.3 (8–2%)	6	17.33 ± 3.37 (9–11%)
CP	1/4 width of CP BW	2.01 ± 0.38 (170%)	4.47 ± 0.64 (129%)	3.49 ± 0.35 (83%)	198.8 ± 10.4 (0%)	228.9 ± 10.8 (2%)	8	14.60 ± 3.22 (8%)
REC	1/4 width of CP BW	2.46 ± 0.37 (231–22%)	5.49 ± 0.77 (181–23%)	4.00 ± 0.40 (110–15%)	198.8 ± 10.4 (12–12%)	229.0 ± 18.8 (4–2%)	4	15.52 ± 3.16 (2–6%)

[1]The values in the table are described in terms of the mean plus/minus one standard deviation. In parentheses: absolute percent change of REC-FC vs. CP reference − absolute percent change of REC-FC vs. CP-FC for the same case.
[2]CP = conventional pulsing; REC = resolution enhancement compression.
[3]BW = bandwidth.

The other cases evaluated were half-, third-, and fourth-width of CP impulse response, which would translate into a reduction by a factor of 2, 3, and 4 in terms of axial resolution, respectively. The half-, third-, and fourth-width case FC filter banks were applied to both CP and REC as shown in Figs. 6(c)–(e). For these cases, unlike the full-width case where the axial resolution was restored to the original axial resolution with dramatic improvements in contrast, a tradeoff between the axial resolution and contrast resolution exists. In fact, it was observed from the lSNR values that as the bandwidth of the subband used in FC became smaller, the loss in axial resolution outweighed the increase in contrast obtained. In the simulations, the lSNR for the fourth-width case when using REC-FC suffered from a significant drop, which is attributed to the deterioration of axial resolution; however, REC-FC was better than CP and CP-FC in terms of lSNR. These improvements in terms of lSNR quantified significant benefits of using REC-FC over CP-FC.

Histograms of the background and target regions for all 4 cases are shown in Fig. 8. From examination of the reference scans in Fig. 8(a), it is apparent that there is a

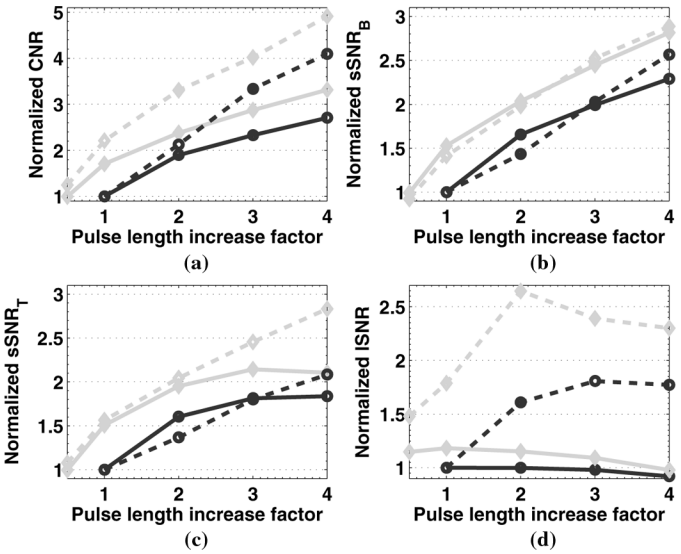

Fig. 5. (a) Normalized CNR vs. pulse length increase factor, (b) normalized sSNR_B vs. pulse length increase factor, (c) normalized sSNR_T vs. pulse length increase factor, (d) normalized lSNR vs. pulse length increase factor. For simulations and experiments, the quality metric values are normalized to the data corresponding to conventional pulsing with a pulse length increase factor of one. (Simulated results are depicted by a solid line, experimental measurements are shown in a dashed line, resolution enhancement compression results are marked by diamonds, and conventional pulsing results are marked by circles).

large overlap in the distribution of gray-scale pixel intensities between the background and the target, which was due to the large spread in the standard deviation about the mean pixel value of these regions. In fact, the overlap of these regions for the CP and REC reference scans was 28%. A large overlap between these 2 regions was undesirable because it would decrease the ability to detect the target from the background. By using FC, the overlap was reduced to 18% for the full-width case as shown in Fig. 8(b). This 10% decrease of overlap can be attributed to a reduction of 11.6 and 11.7 in the standard deviation of pixel intensities about the mean for the background and the target regions, respectively. In addition, as expected, the percent overlap for the half-, third-, and fourth-width for CP-FC cases shown in Figs. 8(c)–(e) decreased; however, the overlap obtained with CP-FC was higher when compared with REC-FC.

IV. Experimental Setup and Results

Experiments were performed to validate the simulated results. A single-element weakly focused (f/2.66) transducer (Panametrics, Waltham, MA) with a center frequency of 2.25 MHz and a 50% (at −3-dB) fractional bandwidth was used to image a phantom by translating the transducer laterally. There were 2 different experimental setups used; one for CP methods and another one for REC experiments. These setups would contain different noise levels due to the use of different excitation systems; therefore, to avoid errors in the comparisons, the noise levels were nor-

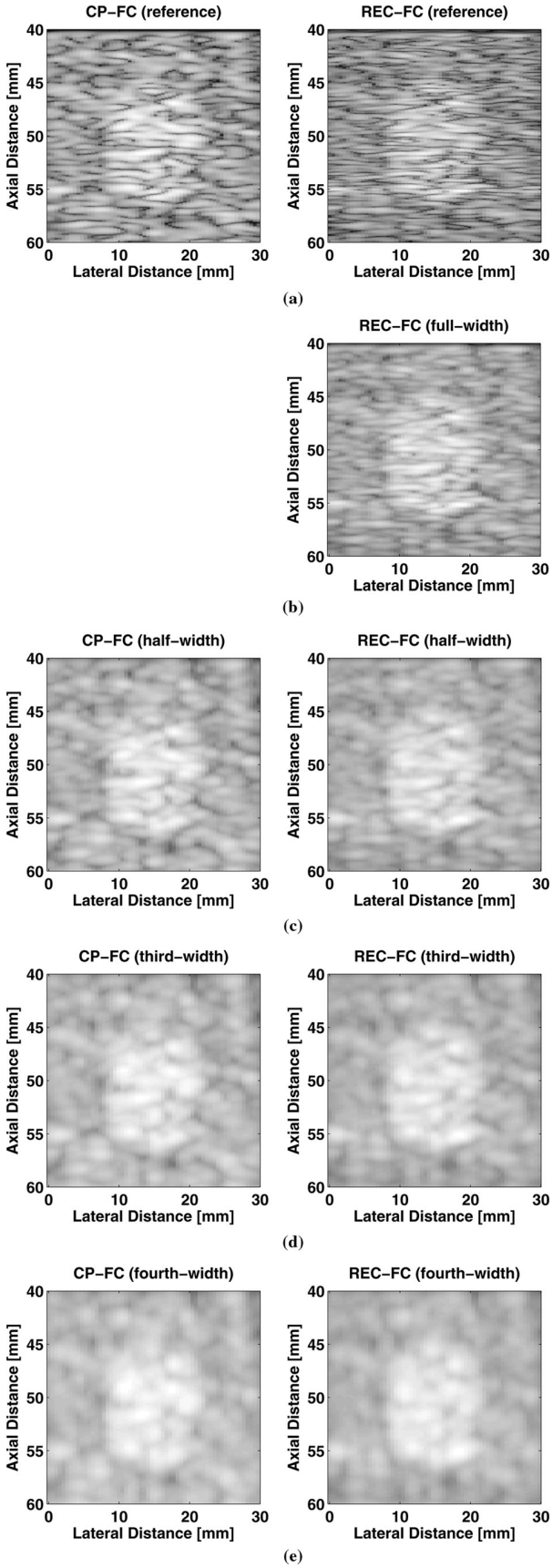

Fig. 6. B-mode images of simulated results for the following: (a) CP and REC reference scans, (b) REC-FC full-width case, (c) CP-FC and REC-FC half-width cases, (d) CP-FC and REC-FC third-width cases, and (e) CP-FC and REC-FC fourth-width cases. Image dynamic range = −50 dB.

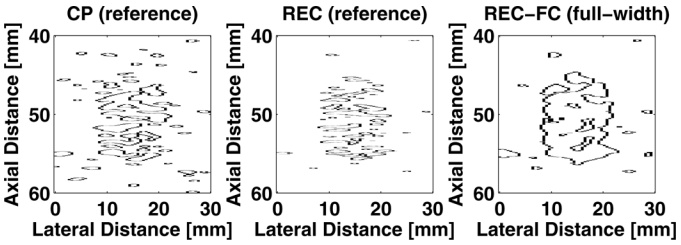

Fig. 7. Edge-detection images of simulated results using thresholding and margin strength for CP, REC, and REC-FC full-width case.

malized to an eSNR of 28 dB. Normalization of eSNR was accomplished by adding zero mean Gaussian white noise to the CP RF echo waveform. The 2 experimental setups are described as follows:

1. Conventional pulsing experimental setup: The transducer was excited by a pulser-receiver (5800, Panametrics, Waltham, MA) and the receive waveform was displayed on an oscilloscope (9354 TM, Lecroy, Chester Ridge, NY) for visual verification. The echo signal was recorded at a rate of 100 MHz by a 12-bit A/D (Digitizing Board UF3025, Strategic Test, Woburn, MA) for further processing by a PC. A diagram of the experimental setup for CP is shown in Fig. 9(a).
2. REC experimental setup: The pre-enhanced chirp was generated in Matlab (MathWorks, Natick, MA) and downloaded to an arbitrary waveform generator (W1281A, Tabor Electronics, Tel Hanan, Israel). The excitation signal was sampled at a rate of 100 MHz and amplified by an RF power amplifier (3251, ENI, Rochester, NY). The amplified signal (50 dB) was connected to the transducer through a diplexer (RDX-6, Ritec Enterprises, Warwick, RI). The echo signal was received by a pulser-receiver (5800, Panametrics, Waltham, MA), which was displayed on an oscilloscope (9354 TM, Lecroy, Chester Ridge, NY) for visual verification. The echo signal was recorded at a rate of 100 MHz by a 12-bit A/D (Digitizing Board UF3025, Strategic Test, Woburn, MA) for further processing by a PC. A diagram of the experimental setup for REC is shown in Fig. 9(b).

A tissue-mimicking phantom (Model 539, ATS Laboratories, Bridgeport, CT) was used to assess the performance of REC-FC with the image quality metrics described in Section II. The material from the tissue-mimicking phantom consisted of urethane rubber, which has a speed of sound of 1450 m/s $\pm$ 1.0% at 23°C and an attenuation coefficient of 0.5 dB/cm/MHz $\pm$ 5.0%. A +6-dB echogenic gray-scale target structure with a 15-mm diameter at a depth of 4 cm was imaged for all 4 cases in addition to the reference signals. All measurements were conducted at room temperature in a tank of degassed water. Furthermore, in experimental measurements, no optimization of the γ parameter in the Wiener filter (2) was used. Also,

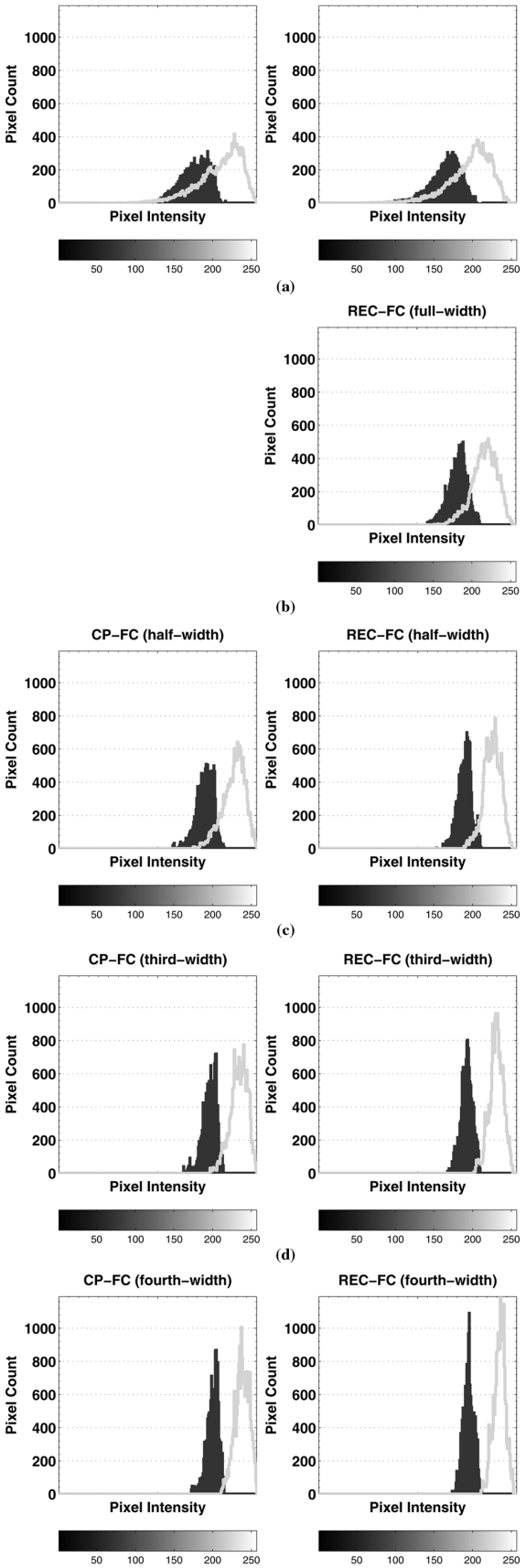

Fig. 8. Histograms of simulated results for the following: (a) CP and REC reference scans, (b) REC-FC full-width case, (c) CP-FC and REC-FC half-width cases, (d) CP-FC and REC-FC third-width cases, and (e) CP-FC and REC-FC fourth-width cases (dark: background region, light: target region).

the same technique to determine the γ as described in Section III was used for the experimental measurements. A description of the filter banks designed along with the resolution needed to calculate lSNR in (9) are shown in Table III. The CNR, sSNR, HPI, HO, and lSNR results obtained for all 4 cases (full-, half-, third-, and fourth-width) in addition to the reference scans (CP and REC with no compounding) are summarized in Table IV. In addition, the improvements in terms of CNR, sSNR_B, and sSNR_T are shown in Figs. 5(a)–(c). The B-mode images representing these results are displayed in Fig. 10.

Examination of the reference scans in Fig. 10(a) reveal that, by using the REC technique, the speckle size was finer when compared with CP, which was evident in the simulations. Next, FC was applied with subbands corresponding to the bandwidth of the original impulse response of the source under CP methods (full-width) to improve contrast as shown in Fig. 10(b). For the full-width case, the CNR, sSNR_B, and sSNR_T using REC-FC improved by a factor of 121%, 41%, and 57% when compared with CP. An increase in CNR and sSNR was obtained while maintaining the same axial resolution that would be obtained by using CP methods. Therefore, the same enhanced definition of object boundaries observed in simulated B-mode images and quantified through the margin strength when using REC leads to better definition of the object boundaries because there is more detail compared with CP. Therefore, when applying REC-FC, this extra information can enhance the results obtained when compared with CP. Evaluating lSNR results shown in Fig. 5 suggest that, by using REC, the lSNR improved by 48% over CP indicating improved target detectability. This would imply that the same lSNR value would be obtained for both CP and REC if a target of approximately 7.8 mm in diameter were imaged with REC rather than 15 mm as in CP.

A comparison of experimental results against simulations reveals the improvement for the full-width case in terms of sSNR_B and sSNR_T remained approximately the same, while the improvement in terms of CNR was larger in the experiment (121%) when compared with simulations (71%). The next case evaluated was half-width of CP impulse response, which consisted of subbands that use half the bandwidth of the impulse response of the source under CP methods. The half-width case was applied to both CP and REC as shown in Fig. 10(c). Comparing experimental results to simulations indicated that the improvements for the half-width case in terms of sSNR_B and sSNR_T were quite similar, while the improvement in terms of CNR was larger in the experiment (231%) when compared with simulations (137%). There are 2 other cases evaluated shown in Figs. 10(d) and (e): third-width and fourth-width. These cases represent a pulse length increase factor of 3 and 4, respectively. For the third- and fourth-width REC-FC cases, the lSNR dropped, but yet maintained higher values than CP, for the third- and fourth-width case with increases of 139% and 130%, respectively. This decrease relates to the visible effects of target edge blurring due to the resolution decrease in B-mode images. Therefore, based on simulation and experimental results, it may not be recommended to drive REC-FC beyond the half-width case.

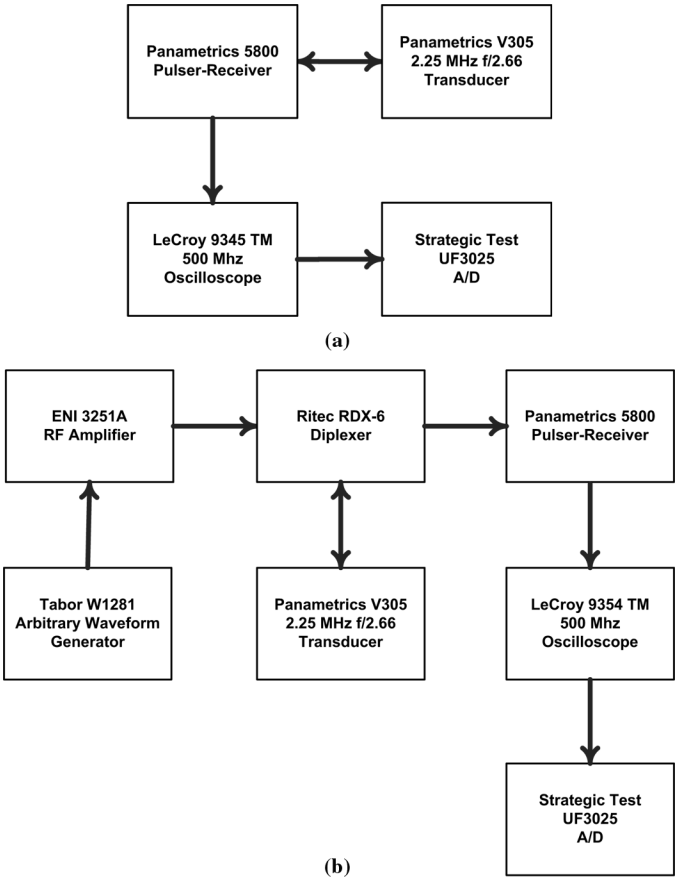

Fig. 9. (a) Block diagram of experimental setup for conventional pulsing and (b) block diagram of experimental setup for resolution enhancement compression.

Histograms of the background and target regions for all 4 cases are shown in Fig. 11. Examination of the reference scans shown in Fig. 11(a) reveal that there is a large overlap in the distribution of gray-scale pixel intensities between the background and the target, which was due to the large spread in the standard deviation about the mean pixel intensity of these regions. In fact, the overlap of these regions for the CP and REC reference scan were both 35%. By using REC-FC, the overlap was reduced to 33% for the full-width case as shown in Fig. 11(b). A major difference between simulations and experiments was that the mean pixel intensity value for the background region increased during simulations while the value decreased for experimental measurements. The mean pixel intensity values for the target increased for both simulation results and experimental measurements. This change in the mean pixel value may help explain how the CNR results improved drastically during experiments compared with simulations. Another factor that may have led to the greater improvement in CNR for experimental measurements versus simulations is the fact that the simulations did not contain noise. In using a coding technique and FC, noise may be further reduced leading to enhanced CNR

TABLE III. FILTER BANK DESCRIPTIONS, AXIAL AND LATERAL CORRELATION FUNCTIONS FOR THE EXPERIMENTAL RESULTS FOR THE 15-MM TARGET FROM THE ATS PHANTOM.

		Filter Banks			Resolution[1]	
Technique[2]	Description	Bandwidth (MHz)	Separation (MHz)	Quantity	Axial (mm)	Lateral (mm)
CP	Reference scan	—	—	—	0.39	1.2
REC	Reference scan	—	—	—	0.21 (46%)	1.2 (0%)
REC-FC	Full width of CP BW[3]	1.2	1.1	4	0.37 (5%)	1.2 (0%)
CP-FC	1/2 width of CP BW	0.6	0.6	3	0.68 (74%)	1.2 (0%)
REC-FC	1/2 width of CP BW	0.6	0.6	6	0.45 (15%)	1.0 (16%)
CP-FC	1/3 width of CP BW	0.4	0.4	6	0.80 (105%)	1.2 (0%)
REC-FC	1/3 width of CP BW	0.4	0.4	10	0.65 (67%)	1.4 (16%)
CP-FC	1/4 width of CP BW	0.3	0.3	10	1.25 (221%)	1.2 (0%)
REC-FC	1/4 width of CP BW	0.3	0.3	15	1.34 (244%)	1.2 (0%)

[1]Values in parentheses represent the absolute percent change of REC-FC vs. CP reference.
[2]CP = conventional pulsing; REC = resolution enhancement compression.
[3]BW = bandwidth.

TABLE IV. CNR, SSNR, HPI, AND LSNR FOR THE EXPERIMENTAL RESULTS FOR THE 15-MM TARGET FROM THE ATS PHANTOM.[1]

Technique[2]	Description	CNR	$sSNR_B$	$sSNR_T$	HPI_B	HPI_T	HO (%)	lSNR
CP	Reference scan	0.33	2.09	1.71	180.0 ± 26.4	193.8 ± 31.5	35	9.9
REC	Reference scan	0.42 (25%)	1.93 (7%)	1.84 (8%)	176.8 ± 27.1 (2%)	193.5 ± 29.6 (0%)	35	14.6 (48%)
REC	Full width of CP BW[3]	0.74 (121%)	2.95 (41%)	2.68 (57%)	158.0 ± 22.5 (12%)	183.1 ± 25.4 (6%)	33	17.6 (78%)
CP	1/2 width of CP BW	0.71 (112%)	2.99 (43%)	2.34 (37%)	174.9 ± 20.0 (3%)	197.4 ± 24.5 (2%)	33	15.0 (52%)
REC	1/2 width of CP BW	1.11 (231–56%)	4.13 (98–38%)	3.49 (104–49%)	159.8 ± 18.1 (11–9%)	190.8 ± 21.3 (2–3%)	28	26.1 (164–74%)
CP	1/3 width of CP BW	1.11 (233%)	4.24 (102%)	3.08 (80%)	161.3 ± 18.8 (10%)	197.0 ± 25.7 (2%)	28	17.8 (80%)
REC	1/3 width of CP BW	1.35 (302–21%)	5.27 (152–24%)	4.20 (146–36%)	139.3 ± 20.0 (23–14%)	182.4 ± 25.0 (6–7%)	21	23.6 (139–33%)
CP	1/4 width of CP BW	1.37 (309%)	5.36 (156%)	3.56 (108%)	157.6 ± 16.9 (12%)	199.5 ± 25.5 (3%)	25	17.5 (78%)
REC	1/4 width of CP BW	1.65 (391–20%)	6.03 (189–13%)	4.84 (183–36%)	138.5 ± 19.6 (23–12%)	190.4 ± 24.8 (2–5%)	19	22.7 (130–30%)

[1]The HPI values in the table are described in terms of the mean plus/minus one standard deviation. In parentheses: absolute percent change of REC-FC vs. CP reference; absolute percent change of REC-FC vs. CP-FC for the same case.
[2]CP = conventional pulsing; REC = resolution enhancement compression.
[3]BW = bandwidth.

over just the compounding effect alone. Furthermore, the overlap for the half-, third-, and fourth-width for CP-FC cases shown in Figs. 11(c)–(e) decreased; however, the overlap obtained with CP-FC is higher when compared with REC-FC. Nonetheless, it should be noted that, although the overlap between these 2 regions was reduced, in addition to the contrast improvements as each FC case was applied, the reduction in axial resolution resulted in deteriorating image quality for the third- and fourth-width cases. This reduction in image quality could reduce the ability to detect small targets. This effect was not as noticeable in the simulation results except for the fourth-width case.

V. DISCUSSION AND CONCLUSION

A pulse-compression and coded-excitation technique, REC, was used to double the axial resolution, which translated into an increase in system bandwidth. The speckle-reduction technique known as FC used this larger available bandwidth to improve image contrast in ultrasonic B-mode images. FC partitions the usable bandwidth by using subbands that are smaller than the system bandwidth to improve image contrast and reduce speckle noise but at the expense of axial resolution. Therefore, the major objective of this study was to establish the benefits of doubling the axial resolution by using REC and applying

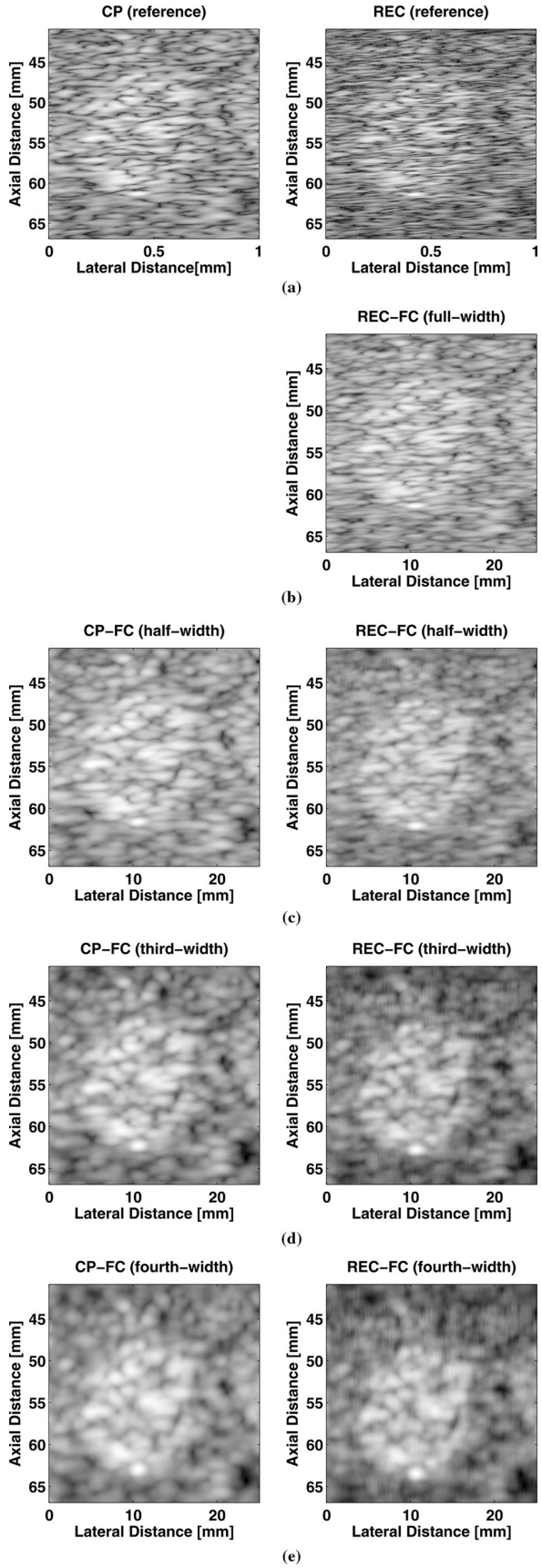

Fig. 10. B-mode images of experimental measurements for the following: (a) CP and REC reference scans, (b) REC-FC full-width case, (c) CP-FC and REC-FC half-width cases, (d) CP-FC and REC-FC third-width cases, and (e) CP-FC and REC-FC fourth-width cases. Image dynamic range = −50 dB.

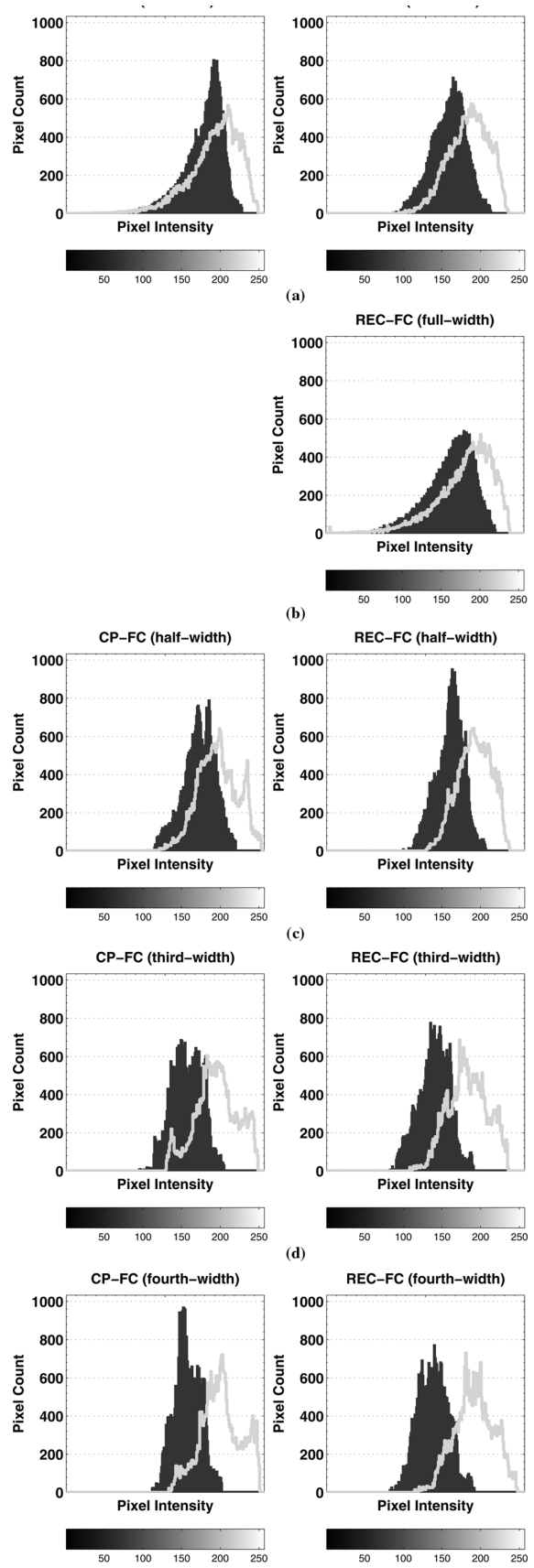

Fig. 11. Histograms of experimental measurements for the following: (a) CP and REC reference scans, (b) REC-FC full-width case, (c) CP-FC and REC-FC half-width cases, (d) CP-FC and REC-FC third-width cases, and (e) CP-FC and REC-FC fourth-width cases (dark: background region, light: target region).

FC to take advantage of the larger usable bandwidth to increase the number of subbands.

Simulations and experimental measurements were used to establish the usefulness of the REC-FC technique in enhancing image contrast and reducing speckle noise. Simulations and experimental measurements suggest that REC-FC was a useful tool to obtain substantial improvements in terms of image contrast and to enhance the boundaries between the target and the background. CNR, $SSNR_B$, and $SSNR_T$ were increased in both simulations and experiments for all cases. Also, in simulations and experiments, the overlap between the background and the target regions in the histograms was significantly reduced as the subbands got smaller. lSNR increased in simulations for all cases except the fourth-width case. However, lSNR from experimental measurements suggested that applying REC-FC for the third- and fourth-width cases might be unfavorable. In general, it appears that REC-FC was always a step ahead of CP/CP-FC. This was due to the doubling of the axial resolution of the ultrasonic-imaging system by using REC, which allowed an increase in the number of subbands.

A potential limitation of the REC-FC technique is the possibility of transducer heating, which may pose a patient safety problem. When transmitting a preenhanced chirp into a transducer, an increase in energy at the inefficient frequency bands of the transducer exists, which could lead to the conversion of electrical energy into heat instead of sound. Future experiments will examine the tradeoffs between exciting sources with preenhanced chirps and additional heating of the transducer. Another drawback of the REC-FC technique as described herein is the length of preenhanced chirp. In this work, a long excitation signal, which was appropriate for the focal number of the utilized source, was used. However, if sources with low focal numbers are used, a long signal duration, i.e., 20 μs, could compromise images for targets near the source. To compensate for this problem, the signal duration must be decreased, but at the expense of decreasing the time-bandwidth product (TBP) [32]. The TBP is important because the eSNR of the compressed waveform is increased by a factor related to the TBP when compared with the uncompressed waveform.

The REC-FC technique does not require an abundance of changes to the hardware infrastructure of a typical ultrasonic imaging system. The main component required would be an arbitrary waveform generator that can output the preenhanced chirp excitation signals. In addition, a digital signal processor is required to compress the received echoes. However, most ultrasonic imaging systems already contain digital signal processors and versions capable of producing arbitrary waveforms on excitation are possible now. An additional experimental cost to using REC-FC in an ultrasonic imaging system is the requirement of acquiring the pulse-echo impulse response of the imaging system. Nonetheless, the pulse-echo impulse response can be easily obtained by placing a known reflector at the focus of the source and exciting with a pulse.

Further studies will examine the REC-FC technique by using a hydrogel phantom with smaller target sizes and lower target contrast values to evaluate the performance as the lesion gets smaller and as the contrast varies. Other work will include a method to quantify the apparent edge enhancement obtained by using REC-FC. Testing the REC-FC technique with a linear array instead of a single-element focused transducer will also be examined in future studies. An additional study of interest would be compounding the REC reference scan with all REC-FC cases evaluated in this investigation. Other studies may include applying a postprocessing speckle-reduction technique such as wavelet despeckling, adaptive filtering, and deconvolution methods to the full-width case of REC-FC. Essentially, the benefits of such techniques will be greatly improved because the starting point in terms of resolution is the same as CP but with improved contrast and less speckle.

Acknowledgment

The authors would like to thank Marko Orescanin, Roberto J. Lavarello, Professor Michael F. Insana, and Professor William D. O'Brien, Jr. from the University of Illinois at Urbana-Champaign for their useful discussions.

References

[1] C. Burckhardt, "Speckle in ultrasound B-Mode scans," *IEEE Trans. Sonics Ultrason.*, vol. SU-25, pp. 1–6, Jan. 1978.

[2] A. Webb, *Introduction to Biomedical Imaging*. Hoboken, NJ: John Wiley & Sons, Inc., 2003, p. 228.

[3] M. S. Patterson and F. S. Foster, "The improvement and quantitative assessment for B-mode images produced by an annular array/cone hybrid," *Ultrason. Imag.*, vol. 5, no. 3, pp. 195–213, Jul. 1983.

[4] J. C. Bamber and C. Daft, "Adaptive filtering for reduction of speckle in ultrasound pulse-echo images," *Ultrasonics*, vol. 24, pp. 41–44, Jan. 1986.

[5] Y. Chen, R. Yin, P. Flynn, and S. Broschat, "Aggressive region growing for speckle reduction in ultrasound images," *Pattern Recognit. Lett.*, vol. 24, no. 4-5, pp. 667–691, Feb. 2003.

[6] D. C. Crawford, D. S. Bell, and J. C. Bamber, "Compensation for the signal processing characteristics of ultrasound B-mode scanners in adaptive speckle reduction," *Ultrasound Med. Biol.*, vol. 19, no. 6, pp. 469–485, 1993.

[7] V. Dutt and J. F. Greenleaf, "Adaptive speckle reduction filter for log compressed B-scan images," *IEEE Trans. Med. Imaging*, vol. 15, pp. 802–813, Dec. 1996.

[8] T. Loupas, W. N. McDicken, and P. L. Allan, "Adaptive weighted median filter for speckle suppression in medical ultrasound images," *IEEE Trans. Circ. Syst.*, vol. 36, no. 1, pp. 129–135, Jan. 1989.

[9] J. A. Jensen and S. Leeman, "Nonparametric estimation of ultrasound pulses," *IEEE Trans. Biomed. Eng.*, vol. 41, pp. 929–936, Oct. 1994.

[10] W. Yeoh and C. Zhang, "Constrained least squares filtering algorithm for ultrasound image deconvolution," *IEEE Trans. Biomed. Eng.*, vol. 53, pp. 2001–2007, Oct. 2006.

[11] O. V. Michailovich and A. Tannenbaum, "Despeckling of medical ultrasound images," *IEEE Trans. Ultrason. Ferroelectr. Freq. Control*, vol. 53, pp. 64–78, Jan. 2006.

[12] Y. Yue, M. M. Croitoru, A. Bidani, J. B. Zwischenberger, and J. W. Clark Jr., "Nonlinear multiscale wavelet diffusion for speckle suppression and edge enhancement in ultrasound images," *IEEE Trans. Med. Imaging*, vol. 25, pp. 297–311, Mar. 2006.

[13] S. K. Jespersen, J. E. Wilhjelm, and H. Sillesen, "Multi-angle compound imaging," *Ultrason. Imaging*, vol. 20, no. 2, pp. 81–102, Apr. 1998.
[14] G. E. Trahey, S. W. Smith, and O. T. von Ramm, "Speckle pattern correlation with lateral aperture translation: experimental results and implications for spatial compounding," *IEEE Trans. Ultrason. Ferroelectr. Freq. Control*, vol. UFFC-33, pp. 257–264, May 1986.
[15] A. R. Groves and R. N. Rohling, "Two-dimensional spatial compounding with warping," *Ultrasound Med. Biol.*, vol. 30, no. 7, pp. 929–942, Jul. 2004.
[16] P. Soler, G. Delso, N. Villain, E. Angelini, and I. Bloch, "Super-resolution spatial compounding techniques with application to 3D breast ultrasound imaging," *Proc. SPIE*, vol. 6147, pp. 281–292, Mar. 2006.
[17] J. G. Abbott and F. L. Thurstone, "Acoustic speckle: Theory and experimental analysis," *Ultrason. Imaging*, vol. 1, pp. 303–324, Oct. 1979.
[18] S. M. Gehlbach and F. G. Sommer, "Frequency diversity speckle processing," *Ultrason. Imaging*, vol. 9, pp. 92–105, Apr. 1987.
[19] P. A. Magnin, O. T. von Ramm, and F. L. Thurstone, "Frequency compounding for speckle contrast reduction in phased array images," *Ultrason. Imaging*, vol. 4, pp. 267–281, Jul. 1982.
[20] H. E. Melton and P. A. Magnin, "A-Mode speckle reduction with compound frequencies and compound bandwidths," *Ultrason. Imaging*, vol. 6, pp. 159–173, Apr. 1984.
[21] V. L. Newhouse, N. M. Bilgutay, J. Saniie, and E. S. Furgason, "Flaw-to-grain echo enhancement by split-spectrum processing," *Ultrason. Imag.*, vol. 4, pp. 59–68, Mar. 1982.
[22] G. E. Trahey, J. W. Allison, S. W. Smith, and O. T. von Ramm, "A quantitative approach to speckle reduction via frequency compounding," *Ultrason. Imaging*, vol. 8, pp. 151–164, Jul. 1986.
[23] F. L. Lizzi, M. E. Elbaum, and E. Feleppa, "Frequency diversity for image enhancement," U.S. Patent 4 561 019, Dec. 24, 1985.
[24] P. F. Stetson, F. G. Sommer, and A. Macovski, "Lesion contrast enhancement in medical ultrasound imaging," *IEEE Trans. Med. Imaging*, vol. 16, pp. 416–425, Aug. 1997.
[25] M. L. Oelze, "Bandwidth and resolution enhancement through pulse compression," *IEEE Trans. Ultrason. Ferroelectr. Freq. Control*, vol. 54, pp. 768–781, Apr. 2007.
[26] J. K. Tsou, J. Liu, and M. F. Insana, "Modeling and phantom studies of ultrasonic wall shear rate measurements using coded excitation," *IEEE Trans. Ultrason. Ferroelectr. Freq. Control*, vol. 53, pp. 724–734, Apr. 2006.
[27] S. W. Smith, R. F. Wagner, J. M. Sandrik, and H. Lopez, "Low contrast detectability and contrast/detail analysis in medical ultrasound," *IEEE Trans. Sonics Ultrason.*, vol. 30, pp. 164–173, May 1983.
[28] S. W. Smith, H. Lopez, and W. J. Bodine Jr., "Frequency independent ultrasound contrast-detail analysis," *Ultrasound Med. Biol.*, vol. 11, no. 3, pp. 467–477, May-Jun. 1985.
[29] R. F. Wagner, S. W. Smith, J. M. Sandrik, and H. Lopez, "Statistics of speckle in ultrasound B-Scans," *IEEE Trans. Sonics Ultrason.*, vol. 30, pp. 156–163, May 1983.
[30] J. A. Jensen, "A model for the propagation and scattering of ultrasound tissue," *J. Acoust. Soc. Am.*, vol. 89, pp. 182–190, Jan. 1991.
[31] P. M. Shankar, V. A. Dumane, C. W. Piccoli, J. M. Reid, F. Forsberg, and B. B. Goldberg, "Computer-aided classification of breast masses in ultrasonic B-scans using a multiparameter approach," *IEEE Trans. Ultrason. Ferroelect. Freq. Contr.*, vol. 50, no. 8, pp. 1002–1009, Aug. 2003.
[32] T. Misaridis and J. A. Jensen, "Use of modulated excitation signals in medical ultrasound. Part I: Basic concepts and expected benefits," *IEEE Trans. Ultrason. Ferroelectr. Freq. Control*, vol. 52, pp. 177–191, Feb. 2005.

Jose R. Sanchez was born in Houston, Texas, in 1977. He earned his B.S. and M.S. degrees in electrical engineering in 2000 and 2002 from Bradley University, Peoria, IL.

Since 2002, Mr. Sanchez has been at Bradley University, where he is an instructor of electrical and computer engineering. As of 2005, Mr. Sanchez is on a leave of absence while he pursues a doctoral degree in electrical engineering at the University of Illinois at Urbana-Champaign. His research interests include ultrasonic imaging, application of coded excitation techniques in ultrasound, and quantitative ultrasound.

Mr. Sanchez is a student member of the IEEE, the IEEE UFFC Society, and a member of the Acoustical Society of America.

Michael L. Oelze was born in Hamilton, New Zealand, in 1971. He earned his B.S. degree in physics and mathematics in 1994 from Harding University, Searcy, AR; his M.S. degree in physics in 1996 from the University of Louisiana at Lafayette, Lafayette, LA; and his Ph.D. degree in physics in 2000 from the University of Mississippi, Oxford, MS.

Dr. Oelze was a postdoctoral fellow at the University of Illinois at Urbana-Champaign from 2000 to 2004, conducting research in ultrasound. His research interests include the acoustic interaction with soil, ultrasound tissue characterization, quantitative ultrasound, ultrasound bioeffects, ultrasound tomography techniques, and application of coded excitation to ultrasound imaging. Currently, Dr. Oelze is an assistant professor at the University of Illinois at Urbana-Champaign.

Dr. Oelze is a member of the IEEE, the IEEE UFFC Society, the American Institute for Ultrasound in Medicine, and the Acoustical Society of America.